Title:

Pneumococcal carriage requires KDM6B, a histone demethylase, for its unique inflammatory signature.

Authors:

Michael G. Connor[1], Emma Patey[1ϕ], Orhan Rasid[1], Laura Barrio[2], Daniel P. Miller[4], Richard J. Lamont[3], Jost Enninga[2], and Melanie A. Hamon[1*]

Affiliations:

[1] Institut Pasteur, G5 Chromatin and Infection, Paris, France

[2] Institut Pasteur, Dynamics of Host-Pathogen Interactions Unit, Paris, France

[3] University of Louisville, Center for Oral Health and Systemic Disease, School of Dentistry, University of Louisville, Louisville, Kentucky, United States of America

[4] Virginia Commonwealth University School of Medicine Dept of Microbiology and Immunology, Richmond, Virginia, United States of America

[ϕ]Current address University of Glasgow, Scotland, UK

* Melanie Hamon (melanie.hamon@pasteur.fr)

Abstract:

Streptococcus pneumoniae (*Sp*), a natural colonizer of the human respiratory tract, is a diverse species with over 90 serotypes. Initial pneumococcal colonization of the human nasopharynx induces two distinct host outcomes; asymptomatic carriage or symptomatic invasive pneumococcal disease depending on the serotype and the host response. Epithelial cells are among the first to encounter both carriage and invasive serotype isolates of pneumococcus. However, the cellular processes responsible for the divergent host responses are largely unknown, as is the contribution of epithelial cells to this process. Here, we show a serotype 6B carriage isolate induces a unique inflammatory signature distinct from invasive serotype 4 (Tigr4). This inflammatory signature is characterized by activation of p65 (RelA) and requires a histone demethylase, KDM6B. At the molecular level, we show that interaction of serotype 6B with epithelial cells leads to chromatin remolding within the IL-11 promoter in a KDM6B dependent manner. We show KDM6B specifically demethylates histone H3 lysine 27 di-methyl, and this facilitates p65 access to three NF-κB sites, which are inaccessible when stimulated by IL-1β or Tigr4. Finally, we demonstrate through chemical inhibition of KDM6B, with GSK-J4 inhibitor, and through exogenous addition of IL-11 that the host response to carriage or invasive phenotypes can be interchanged. Therefore, we demonstrate that epithelial response to either carriage or invasive serotypes of *S. pneumoniae* is divergent and is mediated through chromatin remodeling by KDM6B.

Introduction:

Streptococcus pneumoniae (*Sp*), a clonal species with more than 90 serotypes, naturally colonizes the upper respiratory tract of humans [1-6]. Pneumococcal serotypes are found as either carriage isolates, which are asymptomatic and eventually cleared by the host, or as invasive isolates, which lead to symptomatic disease [5,7,8]. Globally, invasive *S. pneumoniae* is a priority pathogen due to its ability to cause lethal pneumococcal infections resulting from pneumonia, sepsis, or meningitis [4,9]. Importantly, colonization of the nasopharynx is a perquisite for both pneumococcal carriage and invasive disease [2,3,5,10,11].

At these initial colonization events, pneumococcus interacts with the host nasopharyngeal epithelial barrier and the innate immune system. Epithelial cells are among the first responders to pneumococcus and play a pivotal role in dictating pulmonary innate immune responses upon infection[12]. Recent insights using the experimental human pneumococcal carriage (EHPC) model have highlighted the essential role of NF-κB driven inflammatory responses for susceptibility, pathogenesis and transmission of pneumococcus [8,10,13-15]. However, it is still largely unknown how these cellular processes are shaped at the molecular level and result in symptomatic or asymptomatic *S. pneumoniae* infections.

NF-κB is a master transcriptional regulator of both pro- and anti-inflammatory host responses [16-26]. Briefly, NF-κB is comprised of multiple subunits that form hetero- or homodimers, of which the best characterized subunit is p65 (RelA)[27,28]. Activation of p65 occurs through posttranslational modifications (PTMs), such as phosphorylation of serine 536, in response to cellular sensing of inflammatory stimuli (i.e. LPS or interleukin 1 beta (IL-1β)) [28]. Ultimately, activated p65 binds to a kappa-binding consensus sequence site within the nucleus to initiate transcription of NF-κB dependent genes[29]. However, cellular signaling alone is not enough, as a full NF-κB response also requires chromatin remodeling at the targeted inflammatory gene loci [16-26].

Chromatin, is a highly ordered structure of DNA wrapped around histone proteins. Chromatin dynamically shifts between open (euchromatin), and closed (heterochromatin) states, and these states influence gene accessibility and transcription [30-34]. Switching between these two states is the result of chromatin remodeling enzymes/complexes reading, writing and erasing PTMs on histone tails. The enzymes regulating histone PTMs have been identified, and have been shown to play important roles in transcriptional responses during cellular signaling events, such as NF-κB responses [16,35]. One of these enzymes is KDM6B (JMJD3), a histone demethylase, associated with NF-κB. KDM6B belongs to the Jumonji C- domain family (JMJD) of histone demethylases, of which KDM6B is the only member expressed universally outside of embryonic development [24,36]. Primarily through peptide studies, KDM6B

is thought to target the repressive histone marks, lysine 27 tri-methyl (H3K27me3) and di-methyl (H3K27me2) [24,37-39]. To date, mounting evidence, mainly in macrophages, suggests KDM6B is essential for modulating inflammatory gene expression upon wound healing, LPS stimulation and immunological tolerance to anthrax toxin [20-23,40]. However, to our knowledge, no role for KDM6B during bacterial infection has been studied to date.

Herein, we demonstrate a pneumococcal carriage isolate of serotype 6B specifically activates a unique inflammatory signature through p65. This inflammatory signature includes upregulation of KDM6B and IL-11 in human epithelial cells, and these are essential for epithelial cell integrity during challenge with 6B. We demonstrate upon challenge with serotype 6B the promoter of IL-11 is remodeled via KDM6B demethylation of H3K27me2, which allows p65 binding at three NF-κB sites upstream of the IL-11 transcription start site. We demonstrate the importance of this process in regulating epithelial cell integrity as inhibition of KDM6B leads to increased 6B induced epithelial damage; whilst exogenous addition of IL-11 partially rescues serotype 4 (Tigr4) induced cell damage. Thus, we show with chemical inhibition of KDM6B and IL-11, carriage and invasive epithelial-pneumococcal phenotypes can be interchanged.

Results:

Serotype 6B actively induces a unique inflammatory profile.

The differential cellular processes driving the host response during carriage or invasive pneumococcal disease is not entirely known. To address this, we completed an exploratory microarray of human A549 epithelial cells 2hrs post-challenge with either the laboratory invasive strain Tigr4 (serotype 4) or the pneumococcal carriage strain of serotype 6B (clinical isolate; ST90 CC156 lineage F; Fig 1A). In comparison with uninfected cells, 6B differentially influenced 388 transcripts (200 upregulated and 188 downregulated); whilst Tigr4 modulated the expression of 1,205, (143 upregulated and 1,062 downregulated) (Sup. Table1). Strikingly, a large proportion of the total genes differentially regulated by 6B were inflammatory genes containing NF-κB binding sites (12% by 6B vs. 3% by Tigr4; Fig 1B). To confirm this result, we selected a panel of 41 inflammatory genes, including genes from the microarray (*IL-11, KDM6B (JMJD3), PTGS2, CXCL8 (IL8), FOS* and *JUNB*), to test by RT-PCR. Indeed, upon epithelial cell colonization *in vitro*, 6B induced an inflammatory profile, with significantly increased expression of *CSF2 (GM-CSF), CXCL1, CXCL2, CXCL3, IL11, KDM6B* and *TLR9* ($pV \leq 0.05$) in comparison to Tigr4 (Fig. 1C; Sup. Table2). Thus, 6B challenged epithelial cells have a transcriptional profile that is more inflammatory than that of Tigr4.

We further cross-compared the same panel against IL-1β (Sup. Table2), a known pro-inflammatory stimulus activating p65 (RelA). Using the relative expression data obtained from RT-PCR, we performed a principal component (PCA) on the expression values for 6B, Tigr4 and IL-1β (Fig. 1D). Comparative analysis of the biplot of the first two components showed three groups, which accounted for 64.3% of the total variance. This clearly demonstrated 6B was actively inducing a unique inflammatory signature distinct from both Tigr4 and IL-1β. To determine if RT-PCR results reflected protein expression, we preformed immunofluorescence staining for KDM6B, one of the genes differentially expressed, at 2hrs post-challenge (Fig. 1E; Rep. images Sup. Fig. 1A). A549 cells were challenged with either 6B, Tigr4, or paraformaldehyde killed 6B (PFA 6B). Two hours post-challenge the nuclear ratio of KDM6B to DAPI signal intensity was quantified. For 6B there was a significant increase in nuclear KDM6B ($pV \leq 0.001$) compared to Tigr4 and uninfected cells, which mirrored our expression analysis. Furthermore, we did not see a significant increase in nuclear KDM6B following challenge with paraformaldehyde-killed 6B, which suggests that this is an active process due to pneumococcal-epithelial interaction, as paraformaldehyde fixation not only inactivates pneumococcus, but is known to maintain bacterial morphology including pili, and extracellular polymeric substances, such as capsule [41].

To determine whether expression of KDM6B in response to 6B was specific, we tested two additional JMJD methyltransferases (KDM7A and KDM8), and a non-related methyltransferase (EHMT2). KDM6B was the only one to be significantly upregulated by 6B (Sup. Fig. 1B). Together these results show 6B induces a differential transcriptional response in epithelial cells characterized by upregulation of KDM6B.

<u>6B inflammatory profile requires p65 activation and catalytically active KDM6B</u>

A hallmark of inflammatory gene induction is the activation of p65 via phosphorylation at serine 536 (S536)[27]. Thus, we tested if 6B activated p65. Whole cell lysates from 2hrs post-challenge of HeLa GFP-p65 stable cell line were immunoblotted for p65 phosphorylation at S536 (Fig. 2A). In comparison to uninfected cells, both IL-1β (positive control) and challenge with 6B induced p65 phosphorylation of S536 ($pV \leq 0.001$) whereas Tigr4 did not (Fig. 2B). To determine whether p65 activation by 6B had a role in its specific inflammatory signature, we used a chemical inhibitor of p65 activation, BAY 11-7082 [42-44]. A549 cells were pretreated with 10μM BAY 11-7082 3hrs prior to 2hr challenge with 6B, Tigr4 or IL-1β and gene expression in comparison to uninfected cells was determined by RT-PCR. BAY 11-7082 treatment did not affect viability, or gene expression alone in comparison to untreated cells (Sup. Fig. 2A & B; gray bars). We determined expression levels for two genes significantly upregulated by 6B in

comparison to Tigr4, *IL-11* and *KDM6B*, as well as a control gene, *PTGS2*, which is known to be p65 dependent. During 6B challenge no significant effect between untreated (no inhibitor) and DMSO (vehicle control) was observed upon the expression of *PTGS2, IL-11* and *KDM6B*, and under the same conditions *IL-11* and *KDM6B* expression remained roughly two-fold higher on average in comparison to Tigr4 and IL-1β (Fig. 2C; white & light gray bars). In contrast, BAY 11-7082 inhibition of p65 during 6B, Tigr4 or IL-1β challenge resulted in reduction in *PTGS2* across all samples (Fig. 2C; gray bars). Furthermore, the expression of *KDM6B* and *IL-11* were significantly repressed only during 6B challenge in the presence of inhibitor (pV≤0.001 and 0.05 respectfully) in comparison to DMSO treated cells (Fig. 2C; gray bars). These data show p65 activation is required for IL-11 and KDM6B expression upon 6B challenge of epithelial cells.

Previous studies demonstrated KDM6B interacts with p65 for inflammatory gene activation during keratinocyte wound healing, and chIP-seq studies found LPS stimulation of macrophages lead to KDM6B regulation of specific inflammatory genes [21,23]. To determine whether KDM6B had an active role in 6B induced expression of *IL-11* and *KDM6B*, we used GSK-J4, an inhibitor of the catalytic JMJ domain of KDM6B [45]. As a control, we chose expression of *PTGS2*, as it is associated with KDM6B and not H3K27me3, thus inhibition of the catalytic activity of KDM6B should have no effect upon its expression [21]. GSK-J4 (10μM; 24hrs prior) was used to pretreat A549 cells before challenge with 6B, Tigr4 or IL-1β. GSK-J4 alone had no significant effect on cell viability, or gene expression in comparison to untreated cells, nor did it affect the transcripts of *PTGS2*, *IL-11* or *KDM6B* in Tigr4 and IL-1β challenged cells (Fig. 2C and Sup. Fig. 2A & B; black bars). Whereas, when the catalytic activity of KDM6B was inhibited more than a three-fold loss of expression for both *IL-11* and *KDM6B* was observed during 6B challenge compared to DMSO control (Fig. 2C; black bars). GSK-J4 treatment had no effect upon *PTGS2* expression during 6B challenge, demonstrating KDM6B catalytic activity was specifically required for IL-11 expression (Fig. 2C; black bars). With this, we clearly show catalytically active KDM6B is required for 6B induced expression of *IL-11* and *KDM6B*.

<u>6B induces chromatin remodeling of the IL-11 promoter for expression.</u>

Since, KDM6B is a histone modifying enzyme localizing to chromatin, we addressed whether 6B induced expression of *IL*-11 required chromatin remodeling within the IL-11 promoter. We mapped and designed ChIP-qPCR primers to predicted kappa-binding sites within the IL-11 promoter using AliBaba2 software, which curates eukaryotic transcription factor DNA binding motifs from the TRANSFAC® database[46]. Three kappa-binding sites upstream (-2,077bp, -774bp, and -406bp) of the IL-11

transcriptional start site (TSS), and one site downstream (+83bp) were predicted (Fig. 3A). Herein, we obtained chromatin from A549 cells 2hrs post-challenge with either 6B, Tigr4, or IL-1β, and compared the recovery of p65, and KDM6B at these kappa-binding sites within the IL-11 promoter using ChIP-qPCR with and without chemical inhibition of the catalytic activity of KDM6B.

During 6B challenge there was a significant (pV≤0.001) recovery of p65 at kappa-binding sites P6 (~25%), P3 (~20%) and P2 (~10%) in contrast to uninfected conditions (Fig. 3B; 6B dark blue; uninfected white). Furthermore, there was ~15% recovery of KDM6B across the same kappa-binding sites in cells challenged with 6B (Fig. 3C; 6B dark blue; uninfected white). In contrast, there was no recruitment of p65 or KDM6B to the kappa-binding sites in IL-1β or Tigr4 challenged cells (Sup. Fig. 3B & C). Recruitment of p65 and KDM6B to these kappa-binding sites was abolished in the presence of the GSK-J4 inhibitor (Fig. 3B &C; 6B light blue; uninfected gray). This clearly showed during 6B challenge the promoter of IL-11 was rearranged in a manner requiring the catalytic activity of KDM6B.

It has been suggested, mainly through peptide studies, that the enzymatic target of KDM6B is primarily H3K27me3 [39,47]. Thus, we hypothesized the chromatin rearrangement within the IL-11 promoter was a result of KDM6B demethylation of H3K27me3. We used ChIP-qPCR to determine the levels of H3K27me3 and H3, for nucleosome occupancy, across the three kappa-binding sites within the IL-11 promoter. Surprisingly, H3K27me3 was not decreased, in fact there was a slight, but significant (pV≤0.05), increase at the P6 kappa-binding site in comparison to unchallenged cells (Fig. 3D; 6B dark blue; uninfected white). There was no enrichment at any kappa-site during IL-1β or Tigr4 challenge (Sup. Fig. 3D). Furthermore, there were no differences in H3 nucleosome distribution at any of the kappa-binding sites between 6B and uninfected cells (Fig. 3E; 6B dark blue; uninfected white), this was also the case for cells challenged with IL-1β or Tigr4 (Sup. Fig. 3E). In the presence of GSK-J4 the increase of H3K27me3 at the P6 and P2 kappa-binding sites was lost in conjunction with a slight but significant increase in H3 nucleosome recovery at P6 (Fig. 3E & D; 6B light blue; uninfected gray). This data showed during 6B challenge KDM6B was not demethlyating H3K27me3, and this mark seemed to increase across the promoter.

Since our data showed an active role for KDM6B enzymatic activity independent of H3K27me3, we tested another proposed substrate of KDM6B, H3K27me2[38]. Our ChIP results showed challenge with 6B induced loss of H3K27me2 at the P6 (pV≤0.01) and variable levels at the P3 and P2 sites within the IL-11 promoter in comparison to uninfected cells (Fig. 3F; 6B dark blue; uninfected white). Strikingly, when KDM6B enzymatic activity was blocked during 6B challenge demethylation of H3K27me2 was significantly inhibited across all kappa-binding sites (Fig. 3F; 6B light blue; uninfected gray).

Together these data show: 1) upon 6B challenge of epithelial cells the promoter of IL-11 is remodeled through the cooperative role of KDM6B and p65, and 2) KDM6B enzymatic activity is directed toward H3K27me2 and independent of H3K27me3 at these kappa-binding sites.

KDM6B and IL-11 contribute to epithelial cell integrity

We next wanted to address the role of KDM6B during 6B colonization of epithelial cells. Interestingly, previous works demonstrate KDM6B and p65 are both required for keratinocyte wound healing [23]. Using these findings coupled with our own data showing 6B induced KDM6B and p65 recruitment to the IL-11 promoter in epithelial cells, we hypothesized that KDM6B and IL-11 were involved in maintaining epithelial cell integrity during pneumococcal colonization. In order to separate epithelial membrane permeability induced mainly by the pneumolysin toxin, a pore forming cholesterol dependent cytolysin (CDC), from cell death, we coupled the LDH cytotoxicity assay with Trypan blue exclusion. Combining these assays allowed us to separate cells with only damaged plasma membranes, which are permissible to Trypan, from dead cells that also release lactate dehydrogenase[48,49]. Herein, we used Trypan blue exclusion and LDH cytotoxicity assays in the presence of KDM6B inhibitor GSK-J4 (10μM) or DMSO (vehicle control) 24hrs prior to challenge with either Tigr4 or 6B (Fig. 4A). We observed no difference in either epithelial integrity or cell viability between uninfected cells with and without GSK-J4 inhibitor (Fig. 4B &E). Furthermore, epithelial integrity and viability was not compromised during 6B challenge in comparison to uninfected cells (Fig. 4B &E). In contrast, challenge with Tigr4 resulted in ~60% epithelial membrane damage (Fig. 4B), and ~45% cell death (Fig. 4E). Strikingly, inhibition of KDM6B catalytic activity affected epithelial integrity of 6B challenged cells, there was a significant ~20% (pV<=0.001) increase in plasma membrane permeability (Fig. 4B), and ~15% (pV<=0.01) increase in LDH release in comparison to the respective controls (Fig. 4E). These results suggest KDM6B plays a role in cell integrity only upon 6B challenge.

Since KDM6B is necessary for both cell integrity and regulates *IL-11* expression, we further tested the role of IL-11 during pneumococcal colonization of epithelial cells. We next determined if exogenous recombinant human IL-11 was sufficient to rescue epithelial integrity loss seen during Tigr4 challenge. At the time of challenge, the inoculums of Tigr4 and 6B were supplemented with recombinant human IL-11 prior to addition to A549 cells. After 2hrs Trypan blue exclusion and LDH release assays were performed (Fig. 4C-E). IL-11 at the time of Tigr4 challenge partially rescued cell integrity by ~20% (pV<=0.001), in comparison to untreated controls (Fig. 4D). There was no significant effect of exogenous IL-11 on uninfected or 6B challenged cells (Fig. 4D). Furthermore, LDH release

showed exogenous IL-11 lowered Tigr4 cytotoxicity by ~15% (pV<=0.01; Fig. 4E). Together this data shows IL-11 contributes to maintaining epithelial cell integrity during pneumococcal colonization.

Our data suggested the carriage isolate of serotype 6B induced KDM6B and IL-11 to maintain epithelial integrity. We hypothesized other pneumococcal carriage isolates could also induce *IL-11* expression, while invasive ones would not. To test this, we compared additional carriage isolates of either serotype 19A or 19F, and two invasive serotype 1 isolates harboring either a hemolytic or non-hemolytic pneumolysin allele. Isolates of serotype 19A and 19F upregulated *IL-11* expression in A549 epithelial cells in comparison to uninfected cells, whereas the serotype 1 isolates did not (Fig. 4F). To determine if *IL-11* upregulation was specific to pneumococcal carriage isolates, or potentially upregulated by commensal organisms, we tested five additional oral microbiome commensals. Indeed, *Streptococcus gordonii*, *Streptococcus sanguinis*, *Streptococcus oralis*, *Eikenella corrodens* and *Fusobacterium nucleatum* also upregulated the expression of *IL-11* in immortalized gingival keratinocytes (Sup. Fig. 4A). Together, our data show pneumococcal carriage isolates and commensal organisms induce *IL-11* expression upon colonization, suggesting a common response is induced by colonizing bacteria. All together, we show pneumococcal carriage isolate 6B requires active KDM6B during *in vitro* colonization of human epithelial cells to mitigate epithelial cell damage, and IL-11 partially rescues epithelial cell integrity during Tigr4 challenge.

KDM6B is essential for local containment of carriage of 6B *in vivo*

Having defined an essential role for KDM6B during serotype 6B colonization of epithelial cells *in vitro*, we hypothesized local inhibition of KDM6B during 6B colonization of the murine nasal epithelium would promote 6B to escape from the nasopharynx due to loss of epithelium integrity. We challenged mice with 3 - 4x10^6 CFU of either 6B or Tigr4 mixed with either DMSO (vehicle control) or 5mM GSK-J4. The plated inoculums showed no significant effect of DMSO or GSK-J4 on bacterial viability (Sup. Fig. 5). Bacterial burden in the nasal lavage (NL), bronchoalveolar lavage fluid (BALF), lungs, and spleens of mice 24 and 48hrs post-inoculation were quantified by conventional colony forming unit (CFU) enumeration (Fig. 5A & B). Bacterial burdens from 6B and Tigr4 challenged DMSO animals showed on average one log more bacteria across all organs in comparison to Tigr4 by 24hrs (Fig. 5A; 6B light blue; Tigr4 gray). By 48hrs, infection with Tigr4 showed a progression of bacteria towards internal organs. The loosely attached bacteria in the NL and BALF decreased, while the burden in the lung and spleen increased in comparison to 24hrs. However, 6B CFU numbers either remained constant or decreased in all samples (Fig. 5B; 6B light blue). With this data we concluded 6B was primarily contained within the murine nasal

cavity, whereas by 48hrs post-inoculation Tigr4 had escaped the nasopharynx and begun to disseminate from the lungs.

However, the addition of GSK-J4 changed the bacterial distribution of 6B. Indeed, GSK-J4 treated animals challenged with 6B showed increased burden across all samples in comparison to the 6B DMSO control group at 24hrs (Fig. 5A). Additionally, the recovered bacteria from the NL and BALF in the GSK-J4 6B challenged group was not significantly different to the Tigr4 DMSO group (Fig. 5A). However, after 24hrs there was no significant difference in the recovery of Tigr4 from the NL, BALF, lungs or spleens between DMSO or GSK-J4 treated animals (Fig. 5A; Tigr4 DMSO white, Tigr4 GSK-J4 gray). By 48hrs post-challenge 6B GSK-J4 animals maintained a significantly ($pV<=0.05$) high bacterial burden in the BALF compared to 6B DMSO treated animals (Fig. 5B; 6B DMSO light blue, 6B GSK-J4 dark blue). Importantly in animals treated with GSK-J4 6B was recovered from the spleen, an organ which bacteria were mostly undetected in DMSO control animals. GSK-J4 treated animals in the Tigr4 group also showed an increase in bacterial burden at 48hrs post-challenge in the NL, BALF, lung and spleen. Altogether, these data show KDM6B activity is specifically required for containment of 6B during colonization of the murine nasal cavity, and is potentially a negative regulator of Tigr4 dissemination.

Discussion:

Colonization of the nasopharynx is an essential process that precedes asymptomatic pneumococcal carriage or symptomatic pneumococcal disease, with the bacteria first encountering the epithelial barrier [3,5]. The molecular and transcriptional processes that define carriage at this stage are largely unknown. Towards this end, we completed a human microarray of A549 epithelial cells challenged with either 6B or Tigr4 pneumococcal strains. We show the pneumococcal carriage isolate 6B differentially regulated 388 genes, with a primary enrichment for NF-κB associated genes in comparison to Tigr4. A further study of NF-κB signaling demonstrated 6B activated p65, in contrast to Tigr4. Direct comparison of NF-κB regulated genes shows that 6B induced a unique inflammatory signature that included *KDM6B* and *IL-11* expression, in contrast to Tigr4. We demonstrate molecularly that carriage pneumococcus, through the activity of KDM6B, induces remodeling of the IL-11 promoter to reveal three NF-κB sites, which are not accessible during IL-1β or Tigr4 stimulation. Together, this is the first demonstration that pneumococcal carriage remodels chromatin within epithelial cells to support a unique inflammatory signature.

Our findings, in conjunction with recent works by *Weight et* al., support the idea that pneumococcal carriage, in contrast to invasive pneumococcus, is actively inducing a host response to promote confinement to the nasopharynx [15]. Our results strongly suggest KDM6B and its regulation of IL-11 transcription are key components modulating the host-pneumococcal response during colonization by carriage and invasive *S. pneumonie* strains. In both *in vivo* and *in vitro* experiments with chemical inhibition of KDM6B, we were able to interchange carriage and invasive phenotypes through a host driven mechanism. Since KDM6B differentially regulates multiple inflammatory genes we cannot rule out the possibility there are other genes with concurrent or synergistic functions with IL-11. However, our IL-11 rescue experiments with Tigr4 suggest a role for IL-11 in locally maintaining a permissive/tolerogenic epithelial-pneumococcal host response. Interestingly, IL-11 is known to influence mucus production, wound healing of gastric ulcers and resistance of endothelial cells to immune mediated injury [50-53]. Promoting the confinement of a carriage pneumococcal strains within the nasopharynx, is also reflected in our microarray data, as 52 genes associated with wound healing gene ontology were upregulated by 6B in comparison to Tigr4 (Sup. Table 1). Additionally, 39 of the 52 upregulated wound healing genes were also associated with KDM6B and/or H3K27me3 determined from the ChIP-seq studies of macrophages (Sup. Table 1). Therefore, our findings suggest the initial pneumococcal-epithelial cell interaction plays an important role in driving a host response leading to divergent asymptomatic or symptomatic phenotypes during pneumococcal disease. Within this principal, we propose, in contrast to invasive serotypes, that early colonization of nasal epithelium by carriage serotypes actively induces “tolerogenic inflammation” through upregulation of wound healing cascades as a means to counter balance an early deleterious pro-inflammatory host response (i.e. neutrophil influx), thus preserving a prolonged niche within the host. Interestingly, we find that a signature gene, IL-11, was also induced by other pneumococcal carriage isolates and by several commensal organisms, suggesting this is a common response to colonizing bacteria.

The lysine demethylase KDM6B has mainly been characterized in cellular development, however a few studies suggest that this particular histone demethylase also fine-tunes inflammatory responses and wound healing downstream of p65 largely through unknown mechanisms [21-24,54-56]. We are the first to report both a biological and molecular role for KDM6B and H3K27me3/2 in regulation of a specific gene locus, IL-11, during bacterial colonization. Surprisingly, although KDM6B was shown to primarily target H3K27me3 and to a lesser extent H3K27me2[38,39,47], our results suggest KDM6B is selectively demethlyating H3K27me2 and not H3K27me3 at the IL-11 promoter. These results are consistent with previous observations of *Da Santa et al.,* who reported gene regulation by KDM6B independently of

H3K27me3 [21]. With this observation, we hypothesize that KDM6B is differentially regulating inflammatory gene expression through selective demethylation of H3K27me2 through either an unknown regulatory element or posttranslational modifications to KDM6B. Future ChIP-seq and proteomic studies with biological stimuli, such as pneumococcus, will yield substantial insight into possible KDM6B complexes, and the dynamics of H3K27me3/2 in epigenetic control of inflammatory signaling cascades.

Through our study of p65 activation by pneumococcus, we find that serotype 6B activated p65 to similar levels as IL-1β, however, the ensuing transcriptomic responses are very different. Combining these observations with active remodeling of the IL-11 promoter strongly suggests that under 6B stimulation there are additional p65 interacting partners or posttranslational modifications (PTMs), in conjunction with phosphorylation of serine 536. Such data would support a novel biological role for "NF-κB barcode hypothesis", where a signature barcode of PTMs on NF-κB mediates a specific gene expression pattern [57,58]. While we have established a link between p65, KDM6B and *IL-11* expression, identification of the p65 PTMs and interacting partners necessary for the inflammatory signature of 6B will advance our understanding of not only carriage pneumococcal host responses, but also p65 regulation during tolerogenic inflammatory responses.

A meta-analysis conducted by *Brouwer et al.*, highlighted single nucleotide polymorphisms (SNPs) associated with *NFKBIA, NFKBIE,* and *TIRAP* correlated with protection, whereas SNPs within NEMO (*IKBKG)* or IRAK4 associated predominantly with increased susceptibility to disease [59]. Analysis of KDM6B and H3K27me3 ChIP-seq data from LPS stimulated macrophages, shows these protective genes, *NFKBIA, NFKBIE,* and *TIRAP*, are also associated with KDM6B and/or H3K27me3, whilst NEMO and IRAK4 are not [21]. Since *NFKBIA,* and *NFKBIE* are known to inhibit NF-κB through sequestration within the cytoplasm [16,60,61], one could hypothesize KDM6B is a chromatin level negative regulator that balances inflammatory signaling in conjunction with p65 across a unique "p65-KDM6B" axis. In this context, KDM6B serves as the molecular "regulator or brake" responsible for modulating the host response based upon the severity, or degree of inflammatory signal input. This role is evidenced by our *in vivo* studies showing chemical inhibition of KDM6B in *vivo* results in hypervirulence of Tigr4 and the escape of a carriage serotype 6B isolate from the murine nasal cavity.

Overall, our data demonstrates the first biological role of KDM6B in bacterial colonization. We further reveal catalytically active KDM6B is required for host tolerance to pneumococcal carriage isolate 6B. We further show exogenous IL-11 is partially sufficient to rescue Tigr4 induced cell damage in vitro.

357 While we have only begun to scratch the surface of the molecular pathways involved in this process, it is
358 clear characterizing pneumococcal carriage can not only identify new means to combat pneumococcal
359 disease, but reveal new mechanisms involved in commensal organism meditated inflammatory
360 processes.
361
362

363 **Materials and Methods**:

364 Bacterial strains, growth conditions and CFU enumeration. Clinical isolates of serotypes 6B (ST90; CNRP#
365 43494), 19A (ST276; CNRP# 45426) and 1 (non-hemolytic; ST306; CNRP# 43810) were obtained from the
366 Centre National de Référence des Pneumocoques (Emmanuelle Varon; Paris, France). Serotype 19F
367 (BHN100; ST162 Birgitta Henriques Normark, Karolinska Institutet [62]), serotype 4 Tigr4 (Thomas Kohler,
368 Universität Greifswald), and serotype 1 (ST304 hemolytic; M. Mustapha Si-Tahar, Université de Tours).
369 Experimental starters were prepared from frozen master stocks struck on 5% Columbia blood agar
370 plates (Biomerieux Ref# 43041) and grown overnight at 37°C with 5% CO_2 prior to outgrowth in Todd-
371 Hewitt (BD) broth supplemented with 50mM HEPES (Sigma) (TH+H) at 37°C with 5% CO_2 in closed falcon
372 tubes. Midlog bacteria were pelleted, and diluted to $0.6OD_{600}$ /mL in TH+H media supplemented with
373 Luria-Bertani (BD) and 15% glycerol final concentration. Aliquots were made and frozen at -80°C for
374 experiments. All experiments performed with frozen experimental starters of *S. pneumoniae* less than
375 14 days old. For experiments, starters were grown to midlog phase in TH+H broth at 37°C with 5% CO2
376 in closed falcon tubes, pelleted at 1,500xg for 10mins at room temperature (RT), washed in DPBS, and
377 concentrated in 1mL DPBS prior to dilution at desired CFU/mL using $0.6OD_{600}$ /mL conversion factors in
378 either cell culture media or DPBS for animal studies (conversion factors Sup. Table 3). For
379 paraformaldehyde (PFA) killed bacteria the concentrated bacteria prior to dilution was incubated 4%
380 PFA for 30mins at RT, washed in DPBS, and diluted to desired CFU/mL using $0.6OD_{600}$ /mL conversion
381 factors. Bacteria CFU enumeration was determined by 96well dilution plating.
382
383 Cell culture and *In vitro* challenge. A549 human epithelial cells (ATCC ref# CCL-185) were maintained in
384 F12K media (Gibco) supplemented with 1x GlutaMax (Gibco) and 10% heat inactivated fetal calf serum
385 (FCS) at 37°C with 5% CO_2. Stable HeLa GFP-p65 were generated using the sleeping beauty system, and
386 maintained in DMEM supplemented with 1x GlutaMax (Gibco) 10% heat inactivated FCS [63]. A549 or HeLa
387 GFP-p65 cells used until passage 15. For *in vitro* challenge studies, A549 or HeLa GFP-p65 cells were
388 plated in tissue culture treated plates at $2x10^5$ cells (6well; for 72hrs), $5x10^4$ cells (24well; for 48hrs), or
389 $1x10^4$ cells (96well; for 48hrs). Bacterial inoculums diluted in cell culture media was added to cells, and
390 bacterial-epithelial cell contact synchronized by centrifugation at 200xg for 10mins at RT, then moved to
391 37°C with 5% CO_2 for 2hrs. For inhibitor studies, cell culture media was aspirated, and replaced with
392 filter sterilized culture media containing inhibitor volume matched DMSO (Sigma), GSK-J4 (Sigma ref#
393 SML0701), or BAY 11-7082 (Sigma ref# B5556) at 10µM final concentration for 24hrs or 3hrs respectively
394 prior to bacterial addition. Human IL-11 (Miltenyi Biotec ref# 130-094-623) and human IL-1β (Enzo Life

Sciences ref# ALX-522-056) were used at 100 ng/mL and 10 ng/mL final concentration respectively in cell culture media.

Immunofluorescence and Trypan blue bright field microscopy. To quantify nuclear KDM6B, A549 cells were seeded on acid washed and UV treated coverslips in 24well plates as described above, 2hrs post-challenge media was aspirated, cells washed in DPBS, and fixed with 2.5% PFA for 10mins at RT. Coverslips were blocked and permeabilized overnight in 5% BSA 0.5% Tween20. Coverslips were incubated for 1hr at RT with KDM6B (1:500; abcam ref# ab38113) diluted in 5% BSA 0.5% Tween20, washed in 0.5% Tween20, and incubated for 1hr with Alexa Fluor 488 secondary. After secondary, coverslips were washed in 0.5% Tween20 and mounted using Prolong Gold with DAPI (Invitrogen). Confocal microscopy images were acquired on a Ziess axio observer sinning disk confocal. Nuclear KDM6B intensity per cell was quantified within an ROI generated from the DAPI signal in Fiji [64]. For Trypan exclusion microscopy, A549 cells were seeded in 96well plates as described above. 2hrs post-challenge culture media was aspirated, cells washed in DPBS, and Trypan blue (Thermo) added for 10mins at RT. Trypan blue was removed, and cells fixed with 2.5% PFA for 10mins at RT. PFA was removed and fixed cells washed in DPBS prior to imaging on a EVOS FL (Thermo). Trypan positive cells were scored manually as % of total cells in an imaged field.

A549 epithelial microarray. A549 cells were infected as described above, and total RNA harvested using RNeasy kit (Qiagen). RNA quality was confirmed using a Bioanalyzer (Agilent). Affymetrix GeneChip human transcriptome array 2.0 was processed as per manufacturer's instructions. Data was analyzed using TAC 4.0 (Applied Biosystems).

LDH assay. LDH assays were performed on cell culture supernatants as per manufacturer's instructions (Pierce LDH cytotoxicity kit (Thermo ref# 88953). LDH absorbance was read using Cytation 5 (BioTek) at manufacturer's recommended excitation and emissions.

ChIP and ChIP-qPCR. Detailed ChIP buffer components are in supplemental methods. In brief, $8x10^6$ A549 cells were cross-linked in tissue culture plates with 1% formaldehyde for 10mins at RT, then quenched with 130mM glycine for 5mins at RT. Cells were washed in DPBS, gently scraped, and transferred to an eppendorf. Harvested cells were pelleted at 200xg, supernatant aspirated and frozen -20°C. To obtain chromatin, cell pellets were thawed on ice and lysed for 30mins on ice in nuclear

isolation buffer supplemented with 0.2% Triton X-100. Nuclei pelleted, supernatant aspirated and suspended in chromatin shearing buffer for sonication with a Bioruptor (Diagenode) to 200-900bp size. Sheared chromatin was cleared by centrifugation, then sampled for size using 2% agarose gel electrophoresis and quantification using Pico488 (Lumiprobe ref# 42010). ChIP grade antibodies to p65 (L8F6) (CST ref #6956), KDM6B (abcam ref# ab38113), H3K27me3 (abcam ref# ab6002), H3 (abcam ref# ab195277), or H3K27me2 (diagenode ref# C15410046-10) were used at manufacturer's recommended concentrations and bound to DiaMag beads (diagenode ref # C03010021-150) overnight with gentle rotation. Quantified chromatin was diluted to 10µg per immunoprecipitation condition was added to antibody bound DiaMag beads overnight with gentle rotation. Beads were washed with buffers 1-6 (supplemental methods), decrosslinked by boiling for 10mins with 10% Chelex, treated with RNase and proteinase K, then purified using phenol-chloroform extraction followed by isopropanol precipitation. Recovered DNA was suspend in molecular grade water, and 1µL used for Sybr Green reactions as per manufacturer's instructions on a BioRad CFX384 (BioRad). % recovery was calculated as 2 raised to the adjusted input Ct minus IP Ct multiplied by 100. For histone marks, H3K27me3/2, the % recovery was normalized to the % recovery of H3. qPCR primers listed in Sup. Table 3.

RNA isolation and RT-PCR. Total RNA isolated using TRIzol (Life technologies ref#15596-026) extraction method as per manufacturer's recommendations. Recovered RNA was suspended in molecular grade water, nano dropped and 5µg converted to cDNA using Super Script IV as per manufacturer's instructions. cDNA was diluted to 20ng/µL in molecular grade water and 1µL used for Sybr Green reactions as per manufacturer's instructions on a BioRad CFX384 (BioRad). RT-PCR primers listed in Sup. Table 3. Relative expression was calculated by ΔΔCt method to *GapDH* [65].

Immunoblots and quantification. Cell culture media was removed, washed in DPBS and whole cell lysates harvested with Laemmli buffer [66]. Lysates were boiled 10min, and frozen at -20°C. Whole cell lysates were ran on 8% polyacrylamide SDS PAGE gels, transferred to PVDF membrane (BioRad), blocked in 5% BSA, then probed for p65 (CST ref #6956), p65 phosphorylation at serine 536 (CST ref# 3033), or actin AC-15 monoclonal (sigma ref# A5441) as per manufacturer's recommendations. Appropriate secondary-HRP conjugated antibodies were used with clarity ECL (BioRad) developing reagents. Membranes were developed on ChemiDoc Touch (BioRad).

458 *In vivo* animal studies. All protocols for animal experiments were reviewed and approved by the CETEA
459 (Comité d'Ethique pour l'Expérimentation Animale - Ethics Committee for Animal Experimentation) of
460 the Institut Pasteur under approval number Dap170005 and were performed in accordance with
461 national laws and institutional guidelines for animal care and use. Wildtype C57BL/6 female 8-9 week
462 old mice were purchased from Janvier Labs (France). Animals were anesthetized with a ketamine and
463 xylazine cocktail prior to intranasal challenge with 20µL of 3 - $4x10^6$ CFU of Tigr4 or 6B. Bacterial
464 inoculums were made as described above with minor modification. In brief, after $0.6OD_{600}$ bacterial
465 were concentrated and diluted in either filter sterilized DMSO/DPBS or 5mM GSK-J4/DPBS. 24 and 48hrs
466 post-inoculation animals were euthanized by CO_2 affixation. The nasal lavage was obtained by blocking
467 the oropharynx, to avoid leakage into the oral cavity and lower airway, and nares flushed with 500µL
468 DPBS. Bronchoalveolar lavage fluid (BALF), lungs, and spleens were collected and placed in 1mL DPBS
469 supplemented with 2x protease inhibitor cocktail (Sigma ref # P1860). CFU were enumerated as
470 described above on 5µg/mL Gentamicin Columbia Blood agar selection plates.
471
472 Statistical analysis. All experiments, unless otherwise noted, were repeated 2-4 times with the statistical
473 test in figure legends. *P* values were calculated using GraphPad Prism software. For RT-PCR all statistics
474 were calculated on either the ΔΔCt or ΔCt depending on the desired comparison. PCA plots using the
475 "prcomp" function of the base stats package in R on scaled and mean centered log2 transformed data.
476 Microscopy data was collected from analysis of 20-50 cells for nuclear staining, or 200-300 cells for
477 brightfield per biological replicate per group. Animal studies used the minimum number of animals
478 required to reach power based on post-hoc CFU analysis calculated using G*Power software.
479

Supplemental Methods:

AlamarBlue cytotoxicity. A549 cell viability was determined using AlamarBlue (Thermo ref# DAL1025) as previously described [67]. AlamarBlue absorbance was read using Cytation 5 (BioTek) at manufacturer's recommended excitation and emissions.

Oral commensal *in vitro* infection and RT-PCR.

ChIP buffer solutions as follows:

Nuclear Isolation Buffer (NIB)	Chromatin shearing buffer (Buffer C)	SDS dilution buffer (buffer D)
15mM Tris pH 7.5	1% SDS	0.6% Triton X-100
60mM KCl	10mM Tris HCL pH 8.0	0.06% NaDOC
15mM $NaCl_2$	1mM EDTA	150mM NaCl
250mM sucrose	0.5mM EGTA	12mM Tris HCL pH 8.0
1mM $CaCl_2$		1mM EDTA
5mM $MgCl_2$		0.5mM EGTA
Day of use	Day of use	Day of use
1x PhosSTOP	1x PhosSTOP	1x PhosSTOP
10mM Sodium Butyrate	10mM Sodium Butyrate	10mM Sodium Butyrate
0.2mM PMSF	0.2mM PMSF	0.2mM PMSF
1x protease cocktail	1x protease cocktail	1x protease cocktail
1x phosphatase inhibitor cocktail	1x phosphatase inhibitor cocktail	1x phosphatase inhibitor cocktail

10% Chelex	1.25M pH 7.6 Glycine buffer
10g into 100mL miliQ water	46.91g Glycine in 400mL milliQ water
	pH adjusted to 7.6 and QC to 500mL

Wash buffer 1 (isotonic)	Wash buffer 2 (isotonic, ionic charge change)	Wash buffer 3 (high salt dilution)
1% Triton X-100	0.5% NP40	0.7% Triton X-100
0.1% NaDOC	0.5% Triton X-100	0.1% NaDOC
150mM NaC	0.5% NaDOC	250mM NaCl
10mM Tris HCL pH 8.0	150mM NaCl	10mM Tris HCL pH 8.0
	10mM Tris HCL pH 8.0	
Wash buffer 4 (high salt dilution)	Wash buffer 5 (salt dilution)	Wash buffer 6 (TE)
0.5% NP40	0.1% NP40	20mM Tris HCL pH 8.0
0.5% Triton X-100	150mM NaCl	1mM EDTA
250mM LiCl	20mM Tris HCL pH 8.0	
20mM Tris HCL pH 8.0	1mM EDTA	
1mM EDTA		

492

References:

1 Donkor, E. S. Understanding the pneumococcus: transmission and evolution. *Frontiers in cellular and infection microbiology* **3**, 7-7, doi:10.3389/fcimb.2013.00007 (2013).

2 Shak, J. R., Vidal, J. E. & Klugman, K. P. Influence of bacterial interactions on pneumococcal colonization of the nasopharynx. *Trends in microbiology* **21**, 129-135, doi:10.1016/j.tim.2012.11.005 (2013).

3 Weiser, J. N., Ferreira, D. M. & Paton, J. C. Streptococcus pneumoniae: transmission, colonization and invasion. *Nature reviews. Microbiology* **16**, 355-367, doi:10.1038/s41579-018-0001-8 (2018).

4 Pneumococcal vaccines WHO position paper--2012. *Releve epidemiologique hebdomadaire* **87**, 129-144 (2012).

5 Bogaert, D., De Groot, R. & Hermans, P. W. Streptococcus pneumoniae colonisation: the key to pneumococcal disease. *Lancet Infect Dis* **4**, 144-154, doi:10.1016/s1473-3099(04)00938-7 (2004).

6 Henriques-Normark, B., Blomberg, C., Dagerhamn, J., Battig, P. & Normark, S. The rise and fall of bacterial clones: Streptococcus pneumoniae. *Nat Rev Micro* **6**, 827-837 (2008).

7 Kadioglu, A., Weiser, J. N., Paton, J. C. & Andrew, P. W. The role of Streptococcus pneumoniae virulence factors in host respiratory colonization and disease. *Nature reviews. Microbiology* **6**, 288-301, doi:10.1038/nrmicro1871 (2008).

8 Jochems, S. P., Weiser, J. N., Malley, R. & Ferreira, D. M. The immunological mechanisms that control pneumococcal carriage. *PLoS pathogens* **13**, e1006665-e1006665, doi:10.1371/journal.ppat.1006665 (2017).

9 Prevention, U. S. D. o. H. a. H. S. C. f. D. C. a. (ed U.S. Department of Health and Human Services & Centers for Disease Control and Prevention) 114 (CDC, CDC, 2013).

10 Ferreira, D. M. *et al.* Controlled human infection and rechallenge with Streptococcus pneumoniae reveals the protective efficacy of carriage in healthy adults. *American journal of respiratory and critical care medicine* **187**, 855-864, doi:10.1164/rccm.201212-2277OC (2013).

11 Weiser, J. N. The pneumococcus: why a commensal misbehaves. *Journal of molecular medicine (Berlin, Germany)* **88**, 97-102, doi:10.1007/s00109-009-0557-x (2010).

12 Quinton, L. J. & Mizgerd, J. P. Dynamics of lung defense in pneumonia: resistance, resilience, and remodeling. *Annual review of physiology* **77**, 407-430, doi:10.1146/annurev-physiol-021014-071937 (2015).

13 Henriques-Normark, B. & Tuomanen, E. I. The Pneumococcus: Epidemiology, Microbiology, and Pathogenesis. *Cold Spring Harbor perspectives in medicine* **3**, a010215, doi:10.1101/cshperspect.a010215 (2013).

14 Robson, R. L., Reed, N. A. & Horvat, R. T. Differential activation of inflammatory pathways in A549 type II pneumocytes by Streptococcus pneumoniae strains with different adherence properties. *BMC infectious diseases* **6**, 71, doi:10.1186/1471-2334-6-71 (2006).

15 Weight, C. M. *et al.* Microinvasion by Streptococcus pneumoniae induces epithelial innate immunity during colonisation at the human mucosal surface. *Nature communications* **10**, 3060, doi:10.1038/s41467-019-11005-2 (2019).

16 Ghosh, S. & Hayden, M. S. New regulators of NF-kappaB in inflammation. *Nature reviews. Immunology* **8**, 837-848, doi:10.1038/nri2423 (2008).

17 Bhatt, D. & Ghosh, S. Regulation of the NF-kappaB-Mediated Transcription of Inflammatory Genes. *Frontiers in immunology* **5**, 71, doi:10.3389/fimmu.2014.00071 (2014).

18 Dong, J., Jimi, E., Zhong, H., Hayden, M. S. & Ghosh, S. Repression of gene expression by unphosphorylated NF-kappaB p65 through epigenetic mechanisms. *Genes & development* **22**, 1159-1173, doi:10.1101/gad.1657408 (2008).

19 Fujioka, S. *et al.* NF-kappaB and AP-1 connection: mechanism of NF-kappaB-dependent regulation of AP-1 activity. *Molecular and cellular biology* **24**, 7806-7819, doi:10.1128/MCB.24.17.7806-7819.2004 (2004).

20 Das, N. D., Jung, K. H. & Chai, Y. G. The role of NF-kappaB and H3K27me3 demethylase, Jmjd3, on the anthrax lethal toxin tolerance of RAW 264.7 cells. *PloS one* **5**, e9913, doi:10.1371/journal.pone.0009913 (2010).

21 De Santa, F. *et al.* Jmjd3 contributes to the control of gene expression in LPS-activated macrophages. *Embo J* **28**, 3341-3352, doi:10.1038/emboj.2009.271 (2009).

22 De Santa, F. *et al.* The histone H3 lysine-27 demethylase Jmjd3 links inflammation to inhibition of polycomb-mediated gene silencing. *Cell* **130**, 1083-1094, doi:10.1016/j.cell.2007.08.019 (2007).

23 Na, J. *et al.* Histone H3K27 Demethylase JMJD3 in Cooperation with NF-κB Regulates Keratinocyte Wound Healing. *Journal of Investigative Dermatology* **136**, 847-858, doi:https://doi.org/10.1016/j.jid.2015.11.029 (2016).

24 Salminen, A., Kaarniranta, K., Hiltunen, M. & Kauppinen, A. Histone demethylase Jumonji D3 (JMJD3/KDM6B) at the nexus of epigenetic regulation of inflammation and the aging process. *Journal of molecular medicine (Berlin, Germany)* **92**, 1035-1043, doi:10.1007/s00109-014-1182-x (2014).

25 Diermeier, S. *et al.* TNFα signalling primes chromatin for NF-κB binding and induces rapid and widespread nucleosome repositioning. *Genome biology* **15**, 536, doi:10.1186/s13059-014-0536-6 (2014).

26 Lone, I. N. *et al.* Binding of NF-κB to Nucleosomes: Effect of Translational Positioning, Nucleosome Remodeling and Linker Histone H1. *PLoS genetics* **9**, e1003830, doi:10.1371/journal.pgen.1003830 (2013).

27 Christian, F., Smith, E. L. & Carmody, R. J. The Regulation of NF-κB Subunits by Phosphorylation. *Cells* **5**, 12, doi:10.3390/cells5010012 (2016).

28 Oeckinghaus, A. & Ghosh, S. The NF-κB Family of Transcription Factors and Its Regulation. *Cold Spring Harbor perspectives in biology* **1**, a000034, doi:10.1101/cshperspect.a000034 (2009).

29 Wong, D. *et al.* Extensive characterization of NF-κB binding uncovers non-canonical motifs and advances the interpretation of genetic functional traits. *Genome biology* **12**, R70-R70, doi:10.1186/gb-2011-12-7-r70 (2011).

30 Avvakumov, N., Nourani, A. & Côté, J. Histone Chaperones: Modulators of Chromatin Marks. *Molecular cell* **41**, 502-514, doi:https://doi.org/10.1016/j.molcel.2011.02.013 (2011).

31 Bannister, A. J. & Kouzarides, T. Regulation of chromatin by histone modifications. *Cell research* **21**, 381-395, doi:10.1038/cr.2011.22 (2011).

32 Black, J. C. & Whetstine, J. R. Chromatin landscape: Methylation beyond transcription. *Epigenetics* **6**, 13-19, doi:10.4161/epi.6.1.13331 (2011).

33 Hammond, C. M., Stromme, C. B., Huang, H., Patel, D. J. & Groth, A. Histone chaperone networks shaping chromatin function. *Nature reviews. Molecular cell biology* **18**, 141-158, doi:10.1038/nrm.2016.159 (2017).

34 Kouzarides, T. Chromatin modifications and their function. *Cell* **128**, 693-705, doi:10.1016/j.cell.2007.02.005 (2007).

35 Lorch, Y. & Kornberg, R. D. Chromatin-remodeling and the initiation of transcription. *Quarterly reviews of biophysics* **48**, 465-470, doi:10.1017/s0033583515000116 (2015).

36 Markolovic, S. *et al.* Structure–function relationships of human JmjC oxygenases—demethylases versus hydroxylases. *Current Opinion in Structural Biology* **41**, 62-72, doi:https://doi.org/10.1016/j.sbi.2016.05.013 (2016).

37 Burchfield, J. S., Li, Q., Wang, H. Y. & Wang, R.-F. JMJD3 as an epigenetic regulator in development and disease. *The international journal of biochemistry & cell biology* **67**, 148-157, doi:10.1016/j.biocel.2015.07.006 (2015).

38 Hong, S. *et al.* Identification of JmjC domain-containing UTX and JMJD3 as histone H3 lysine 27 demethylases. *Proceedings of the National Academy of Sciences of the United States of America* **104**, 18439-18444, doi:10.1073/pnas.0707292104 (2007).

39 Xiang, Y. *et al.* JMJD3 is a histone H3K27 demethylase. *Cell research* **17**, 850-857, doi:10.1038/cr.2007.83 (2007).

40 Satoh, T. *et al.* The Jmjd3-Irf4 axis regulates M2 macrophage polarization and host responses against helminth infection. *Nature immunology* **11**, 936-944, doi:10.1038/ni.1920 (2010).

41 Chao, Y. & Zhang, T. Optimization of fixation methods for observation of bacterial cell morphology and surface ultrastructures by atomic force microscopy. *Applied microbiology and biotechnology* **92**, 381-392, doi:10.1007/s00253-011-3551-5 (2011).

42 Pierce, J. W. *et al.* Novel inhibitors of cytokine-induced IkappaBalpha phosphorylation and endothelial cell adhesion molecule expression show anti-inflammatory effects in vivo. *The Journal of biological chemistry* **272**, 21096-21103 (1997).

43 Karin, M. The beginning of the end: IkappaB kinase (IKK) and NF-kappaB activation. *The Journal of biological chemistry* **274**, 27339-27342 (1999).

44 Gilmore, T. D. The Rel/NF-kappaB signal transduction pathway: introduction. *Oncogene* **18**, 6842-6844, doi:10.1038/sj.onc.1203237 (1999).

45 Kruidenier, L. *et al.* A selective jumonji H3K27 demethylase inhibitor modulates the proinflammatory macrophage response. *Nature* **488**, 404, doi:10.1038/nature11262

https://www.nature.com/articles/nature11262#supplementary-information (2012).

46 Wingender, E. Compilation of transcription regulating proteins. *Nucleic acids research* **16**, 1879-1902, doi:10.1093/nar/16.5.1879 (1988).

47 Agger, K. *et al.* UTX and JMJD3 are histone H3K27 demethylases involved in HOX gene regulation and development. *Nature* **449**, 731-734, doi:10.1038/nature06145 (2007).

48 Walev, I. *et al.* Resealing of large transmembrane pores produced by streptolysin O in nucleated cells is accompanied by NF-kappaB activation and downstream events. *FASEB journal : official publication of the Federation of American Societies for Experimental Biology* **16**, 237-239, doi:10.1096/fj.01-0572fje (2002).

49 Tran, S.-L., Puhar, A., Ngo-Camus, M. & Ramarao, N. Trypan blue dye enters viable cells incubated with the pore-forming toxin HlyII of Bacillus cereus. *PloS one* **6**, e22876-e22876, doi:10.1371/journal.pone.0022876 (2011).

50 Nishina, T. *et al.* Interleukin-11 links oxidative stress and compensatory proliferation. *Sci Signal* **5**, ra5, doi:10.1126/scisignal.2002056 (2012).

51 Wen, C.-Y. *et al.* IL-11 up-regulates Tie-2 expression during the healing of gastric ulcers in rats. *World journal of gastroenterology* **9**, 788-790, doi:10.3748/wjg.v9.i4.788 (2003).

52 Mahboubi, K., Biedermann, B. C., Carroll, J. M. & Pober, J. S. IL-11 Activates Human Endothelial Cells to Resist Immune-Mediated Injury. *The Journal of Immunology* **164**, 3837-3846, doi:10.4049/jimmunol.164.7.3837 (2000).

53 Lee, C. G. *et al.* Endogenous IL-11 signaling is essential in Th2- and IL-13-induced inflammation and mucus production. *American journal of respiratory cell and molecular biology* **39**, 739-746, doi:10.1165/rcmb.2008-0053OC (2008).

632 54 Ohguchi, H. *et al.* KDM6B modulates MAPK pathway mediating multiple myeloma cell growth
633 and survival. *Leukemia* **31**, 2661, doi:10.1038/leu.2017.141

634 https://www.nature.com/articles/leu2017141#supplementary-information (2017).
635 55 Chen, S. *et al.* The histone H3 Lys 27 demethylase JMJD3 regulates gene expression by impacting
636 transcriptional elongation. *Genes & development* **26**, 1364-1375, doi:10.1101/gad.186056.111
637 (2012).
638 56 Young, M. D. *et al.* ChIP-seq analysis reveals distinct H3K27me3 profiles that correlate with
639 transcriptional activity. *Nucleic acids research* **39**, 7415-7427, doi:10.1093/nar/gkr416 (2011).
640 57 Moreno, R., Sobotzik, J.-M., Schultz, C. & Schmitz, M. L. Specification of the NF-κB transcriptional
641 response by p65 phosphorylation and TNF-induced nuclear translocation of IKKε. *Nucleic acids*
642 *research* **38**, 6029-6044, doi:10.1093/nar/gkq439 (2010).
643 58 Collins, P. E., Mitxitorena, I. & Carmody, R. J. The Ubiquitination of NF-κB Subunits in the Control
644 of Transcription. *Cells* **5**, 23, doi:10.3390/cells5020023 (2016).
645 59 Brouwer, M. C. *et al.* Host genetic susceptibility to pneumococcal and meningococcal disease: a
646 systematic review and meta-analysis. *Lancet Infect Dis* **9**, 31-44, doi:10.1016/s1473-
647 3099(08)70261-5 (2009).
648 60 Li, Z. & Nabel, G. J. A new member of the I kappaB protein family, I kappaB epsilon, inhibits RelA
649 (p65)-mediated NF-kappaB transcription. *Molecular and cellular biology* **17**, 6184-6190,
650 doi:10.1128/mcb.17.10.6184 (1997).
651 61 Scherer, D. C., Brockman, J. A., Chen, Z., Maniatis, T. & Ballard, D. W. Signal-induced degradation
652 of I kappa B alpha requires site-specific ubiquitination. *Proceedings of the National Academy of*
653 *Sciences of the United States of America* **92**, 11259-11263, doi:10.1073/pnas.92.24.11259
654 (1995).
655 62 Sandgren, A. *et al.* Virulence in mice of pneumococcal clonal types with known invasive disease
656 potential in humans. *The Journal of infectious diseases* **192**, 791-800, doi:10.1086/432513
657 (2005).
658 63 Kowarz, E., Loscher, D. & Marschalek, R. Optimized Sleeping Beauty transposons rapidly
659 generate stable transgenic cell lines. *Biotechnology journal* **10**, 647-653,
660 doi:10.1002/biot.201400821 (2015).
661 64 Schindelin, J. *et al.* Fiji: an open-source platform for biological-image analysis. *Nature methods* **9**,
662 676-682, doi:10.1038/nmeth.2019 (2012).
663 65 Livak, K. J. & Schmittgen, T. D. Analysis of relative gene expression data using real-time
664 quantitative PCR and the 2(-Delta Delta C(T)) Method. *Methods (San Diego, Calif.)* **25**, 402-408,
665 doi:10.1006/meth.2001.1262 (2001).
666 66 Laemmli, U. K. Cleavage of Structural Proteins during the Assembly of the Head of Bacteriophage
667 T4. *Nature* **227**, 680-685, doi:10.1038/227680a0 (1970).
668 67 Connor, M. G. *et al.* Yersinia pestis Targets the Host Endosome Recycling Pathway during the
669 Biogenesis of the Yersinia Containing Vacuole To Avoid Killing by Macrophages. *mBio* **9**, e01800-
670 01817, doi:10.1128/mBio.01800-17 (2018).

671

672

673 **Author Contributions:**

674 Conceived and designed all experiments: MGC and MAH. Preformed experiments: MGC, EP
675 (KDM6B microscopy and HeLa GFP-p65 western blot), and OR (animal studies). Analyzed data: MGC and
676 EP. DPM performed all oral commensal infections and RT-PCR. LB generated the stable HeLa GFP-p65
677 cell line under the supervision of JE. MGC wrote the original manuscript draft. MGC and MAH edited and
678 reviewed the manuscript. MAH supervised the research. All authors approved the final manuscript.
679

680 **Acknowledgments:**

681 We would like to thank Emmanuelle Varon, Birgitta Henriques Normark, M. Mustapha Si-Tahar,
682 and Thomas Kohler for their generous gifts of *S. pneumonie* strains. We are thankfully Gregory Dore
683 (Institut Pasteur, Nuclear Organization and Oncogenesis Group – Oliver Bischof) for processing the
684 microarray Affymetrix GeneChips. Biostatistics and R discussions with Jose Nabuco (Institute Pasteur)
685 and Jeremy Camp (University of Veterinary Medicine Vienna) were greatly appreciated. Michael G.
686 Connor is support by the Pasteur Foundation Fellowship. G5 Chromatin and infection is support by the
687 Institut Pasteur, and the Agence National de la Recherche (ANREpiBActIn).
688

689 **Conflict of interest statement:**

690 The authors declare no conflict of interest.
691

692 **Figure Legends and Tables:**

693 **Figure 1:** *Carriage serotype 6B induces a unique inflammatory signature*. Human microarray of epithelial
694 A549 cells 2hrs post-challenge (MOI 20) with either 6B (blue) or Tigr4 (gray). Circled 6B genes are NF-κB
695 associated. A) All genes differentially regulated by ± 1.5 fold-change to uninfected condition. B)
696 Comparison of genes identified by microarray containing NF-κB sites between 6B and Tigr4. C) RT-PCR
697 validation of inflammatory genes from cells collected 2hrs post-challenge with either Tigr4 or 6B. Heat
698 map represents fold change to uninfected condition (n=4). Student's T-Test 6B to Tigr4, *= pV≤0.05. IL-
699 11 and KDM6B highlighted in red are unique to 6B dataset. D) Principal component analysis of
700 inflammatory RT-PCR panel (n=4) comparing IL-1β (red), Tigr4 (gray) and 6B (blue). Bioplot of the mean
701 centered and $\log_2$ transformed expression data using the first two components and 60% concentration
702 ellipses around each group. E) Quantification of immunofluorescence microscopy of A549 cells 2hrs
703 post-challenge with either Tigr4, 6B or paraformaldehyde fixed 6B for nuclear staining of KDM6B
704 normalized to DAPI (n=4; 20-50 cells per replicate and group). Tukey box and whisker plot. One way-
705 ANOVA with Tukey's multiple comparison post-hoc test, ***= pV≤0.001.
706
707 **Figure 2:** *Expression of KDM6B and IL-11 is specific to 6B and requires p65 activation*. Immunoblot of
708 stable HeLa p65-GFP expressing cells. Whole cell lysates 2hrs post-challenge with either IL-1β (10
709 ng/mL), Tigr4 (MOI 20), or 6B (MOI 20) and probed for p65, phosphorylated p65 at Serine 536 and actin.
710 A) Representative image of immunoblot. B) Actin normalized ratio phos-p65 S536 to total p65 (n=3). Bar
711 graph ± STD. One way-ANOVA with Tukey's multiple comparison post-hoc test, **= pV≤0.01, ***=
712 pV≤0.001. C) Total RNA 2hrs post-challenge with 6B, Tigr4 or IL-1β was harvested from A549 cells
713 treated with either 10μM BAY 11-7082, 10μM GSK-J4, or DMSO vehicle control (n=4). Transcript levels
714 for *PTGS2, IL-11* and *KDM6B* determined by RT-PCR. Bar graph ± Std. Student's T-Test to untreated, *=
715 pV≤0.05, **= pV≤0.01, ***= pV≤0.001.
716
717 **Figure 3:** *6B induces IL-11 promoter rearrangement*. Chromatin was obtained from untreated (blue) and
718 10μM GSK-J4 (light blue) treated A549 cells 2hrs post-challenge with 6B in comparison to uninfected
719 (untreated white; treated gray). 10 μg chromatin input used for ChIP of p65, KDM6B, H3K27me3 and
720 histone H3 (H3), followed by ChIP-qPCR at locations (P6, P3 & P2) spanning the NF-κB sites upstream of
721 the transcriptional start site (TSS). A) Schematic of IL-11 promoter with ChIP-qPCR primer locations (P6,
722 P3 & P2) and NF-κB sites. B - F) % recovery of input for p65 (B), KDM6B (C), H3K27me3 normalized to H3
723 (D), H3K27me2 normalized to H3 (F), or H3 (E) bound at P6, P3 & P2 in untreated and GSK-J4 treated

samples (n=3 untreated; n=2 GSK-J4 treated). Tukey box and whisker plot with dots representing outliers. Student's T-Test comparisons for untreated to GSK-J4 treated or 6B infected to uninfected, *= pV≤0.05, **= pV≤0.01, ***= pV≤0.001, ns=not significant.

Figure 4: *KDM6B and IL-11 contribute to epithelial cell integrity in response to pneumococcus.* A549 cells untreated or treated with 10µM GSK-J4 or 500ng/mL recombinant human IL-11 prior to 2hr challenge with either Tigr4 or 6B. Post-challenge cells are incubated with Trypan blue for cell integrity, fixed with 2.5% paraformaldehyde and imaged with a brightfield microscope. A) Representative image of GSK-J4 treated A549 cells post 2hr challenge. Scale = 100µM. B) % Trypan positive cells between untreated and GSK-J4 treated (pink) (n=4; 200-300 cells per replicate and group). Uninfected white, Tigr4 gray and 6B blue. Tukey box and whisker plot. C) Representative image of IL-11 treated A549 cells post 2hr challenge. Scale = 100µM. D) % Trypan positive cells between untreated and IL-11 treated (green) (n=4; 200-300 cells per replicate and group). Uninfected white, Tigr4 gray and 6B blue. Tukey box and whisker plot. E) % Cytotoxicity (LDH release) from A549 supernatants 2hrs post-challenge (n=4; 2-3 technicals per replicate). Bar graph ± Std. F) Total RNA harvested from A549 cells 2hrs post-challenge with isolates of serotypes 6B, 19F, 19A, and two isolates of 1 (hemolytic and non-hemolytic Ply). Relative expression of *IL-11* to uninfected cells. All data analyzed by One way-ANOVA with Tukey's multiple comparison post-hoc test, **= pV≤0.01, ***= pV≤0.001, ns=not significant.

Figure 5: *KDM6B is required for host response to serotype 6B.* C57B6 mice (~9weeks) were challenged intranasally with 3 - 4x10^6 CFU of Tigr4 or 6B supplemented with either DMSO (vehicle control) or 5mM GSK-J4. At indicated endpoints bacterial load was enumerated by conventional CFU counts on 5µg/mL Gentamicin Columbia Blood agar selection plates from the nasal lavage (NL), bronchoalveolar lavage fluid (BALF), lungs, and spleen of infected animals. DMSO Tigr4 white, GSK-J4 Tigr4 gray, DMSO 6B light blue, GSK-J4 6B dark blue. A) 24hrs post-inoculation CFU burden of indicated samples (n=10). B) 48hrs post-inoculation CFU burden of indicated samples (n=4). Tukey box and whisker plot with dots representing outliers. One way-ANOVA non-parametric Kruskal-Wallis with Dunn's multiple comparison post-hoc test, *= pV≤0.05, **= pV≤0.01, ***= pV≤0.001, ns=not significant. CFU=colony forming unit. Dotted lines =Limit of detection (LD). LD for each organ: NL (50 CFU); BALF, Lung and Spleen (1000 CFU).

Supplemental Figure 1: *KDM6B microscopy and demethylase RT-PCR.* A) Representative images of nuclear KDM6B (green) merged with nucleus stained with DAPI (false colored red for visual display).

Scale = 10µm. B) Total RNA 2hrs post-challenge with 6B or Tigr4 from A549 cells. Demethylase panel RT-PCR shown as ΔCt (n=3; 3 technicals per biological replicate). Bar graph ± Std. All data analyzed by One way-ANOVA with Tukey's multiple comparison post-hoc test, **= pV≤0.01, ns=not significant.

Supplemental Figure 2: *Tigr4 and IL-1β inhibitor RT-PCR with viability data.* A549 cells untreated or treated with 10µM BAY 11-7082, 10µM GSK-J4, or DMSO vehicle control (n=4). A) Cell viability determined by AlamarBlue. Expressed as % of untreated cells. No significant difference observed. B) Transcript levels for *IL-11*, *KDM6B* and *PTGS2* determined by RT-PCR. Displayed as ΔCt for comparison to untreated (n=4). Bar graph ± Std. All data analyzed by One way-ANOVA with Tukey's multiple comparison post-hoc test, no significant difference observed.

Supplemental Figure 3: *ChIP-PCR IL-11 locus for Tigr4 and IL-1β.* Chromatin obtained from untreated and 10µM GSK-J4 treated A549 cells 2hrs post-challenge with Tigr4 or IL-1β. 10 µg chromatin input used for ChIP of p65, KDM6B, H3K27me3 and histone H3 (H3), followed by ChIP-qPCR at primer locations (P6, P3 & P2) spanning the NF-κB sites upstream of the transcriptional start site (TSS). A) Schematic of IL-11 promoter with ChIP-qPCR primer locations (P6, P3 & P2) and the NF-κB sites. B - E) % recovery of input for p65, KDM6B, H3K27me3 normalized to H3, or H3 bound at P6, P3 & P2 in untreated and GSK-J4 treated samples (n=3 untreated; n=2 GSK-J4 treated. Tukey box and whisker plot with dots representing outliers. No significant difference observed in comparison to 6B or uninfected cells from Fig. 3.

Supplemental Figure 4: *IL-11 RT-PCR with oral commensals.* A) Total RNA harvested from immortalized gingival keratinocytes challenged with *S. gordonii*, *S. sanguinis*, *S. oralis*, *E. corrodens* or *F. nucleatum*. Transcript levels for *IL-11* determined by RT-PCR and represented as relative expression to uninfected (n=1).

Supplemental Figure 5: *Tigr4 and 6B bacterial inoculates from animal challenges.* Tigr4 and 6B inoculums for animal intranasal challenge model in DMSO (vehicle control) or 5mM GSK-J4 (n=2). Conventional CFU enumeration shows no significant difference. Analyzed by One way-ANOVA with Tukey's multiple comparison post-hoc test, ns=not significant.

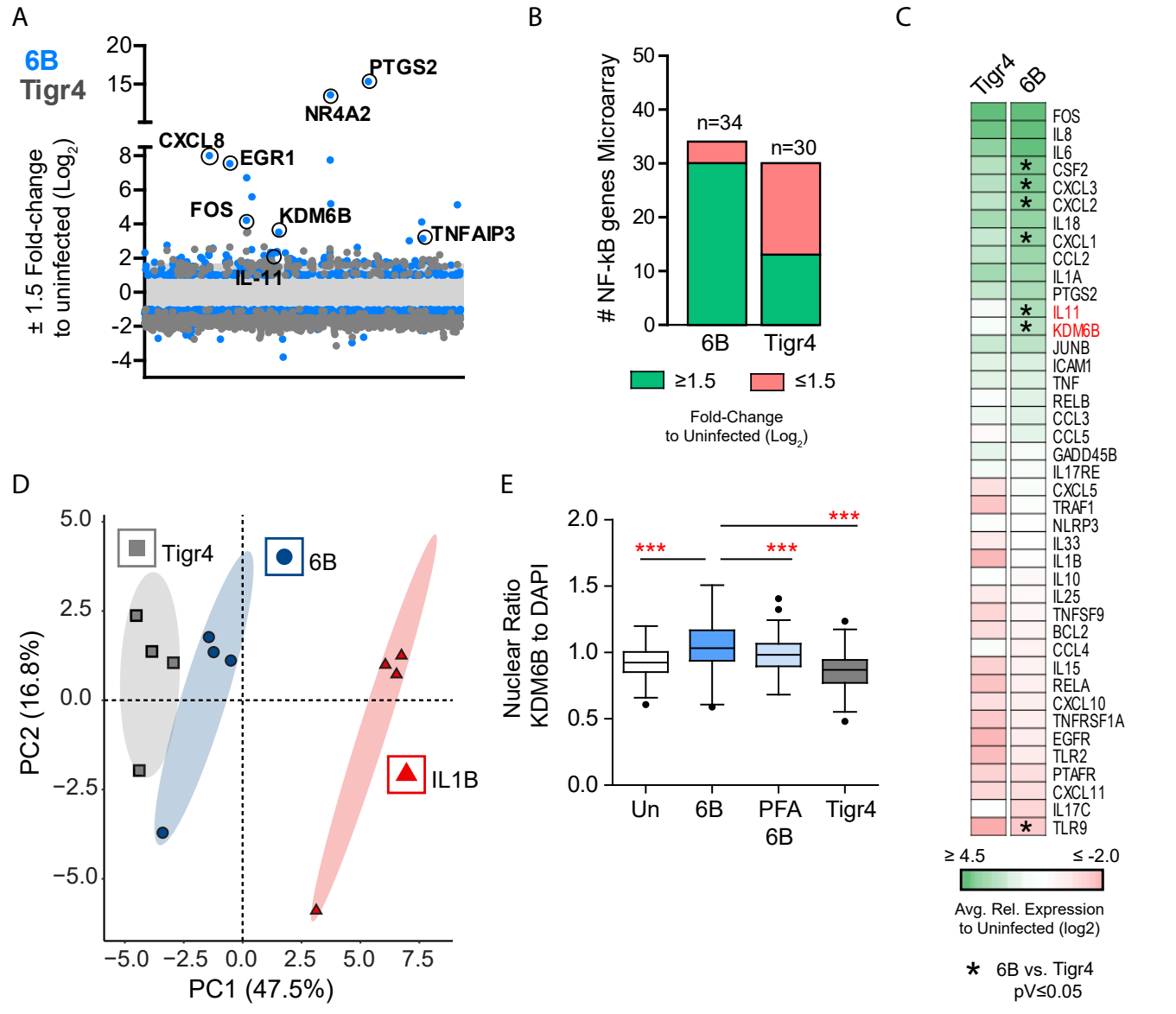
A
6B
Tigr4
± 1.5 Fold-change to uninfected (Log2)
PTGS2
NR4A2
CXCL8
EGR1
FOS
KDM6B
TNFAIP3
IL-11
B
# NF-kB genes Microarray
n=34
n=30
6B
Tigr4
≥1.5
≤1.5
Fold-Change to Uninfected (Log2)
C
Tigr4
6B
FOS
IL8
IL6
CSF2
CXCL3
CXCL2
IL18
CXCL1
CCL2
IL1A
PTGS2
IL11
KDM6B
JUNB
ICAM1
TNF
RELB
CCL3
CCL5
GADD45B
IL17RE
CXCL5
TRAF1
NLRP3
IL33
IL1B
IL10
IL25
TNFSF9
BCL2
CCL4
IL15
RELA
CXCL10
TNFRSF1A
EGFR
TLR2
PTAFR
CXCL11
IL17C
TLR9
≥ 4.5
≤ -2.0
Avg. Rel. Expression to Uninfected (log2)
* 6B vs. Tigr4 pV≤0.05
D
PC2 (16.8%)
PC1 (47.5%)
Tigr4
6B
IL1B
E
Nuclear Ratio KDM6B to DAPI
***
***
***
Un
6B
PFA 6B
Tigr4

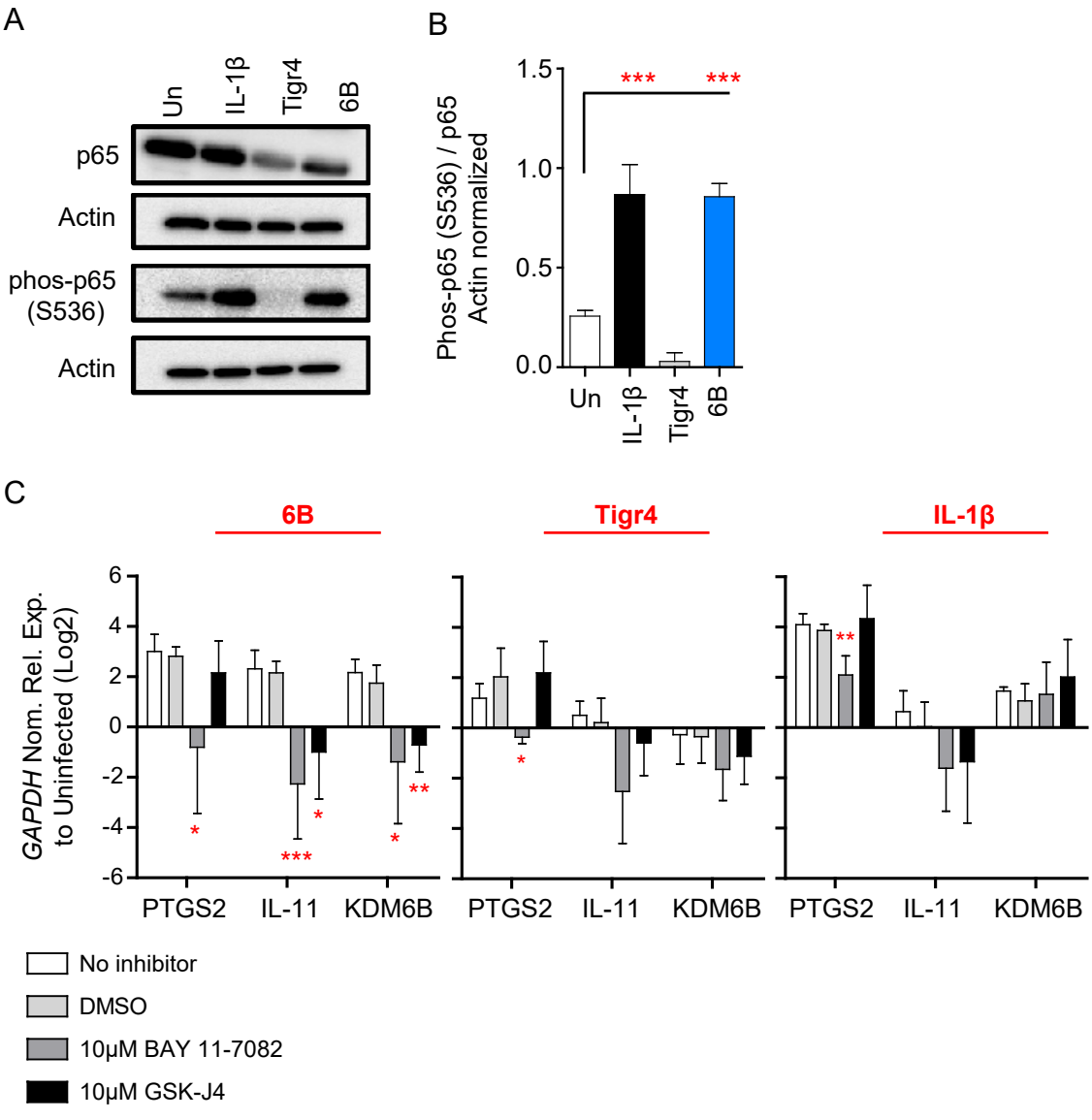
A
Un
IL-1β
Tigr4
6B
p65
Actin
phos-p65 (S536)
Actin
B
Phos-p65 (S536) / p65 Actin normalized
1.5
1.0
0.5
0.0
***
***
Un
IL-1β
Tigr4
6B
C
6B
Tigr4
IL-1β
GAPDH Nom. Rel. Exp. to Uninfected (Log2)
6
4
2
0
-2
-4
-6
PTGS2
IL-11
KDM6B
No inhibitor
DMSO
10μM BAY 11-7082
10μM GSK-J4

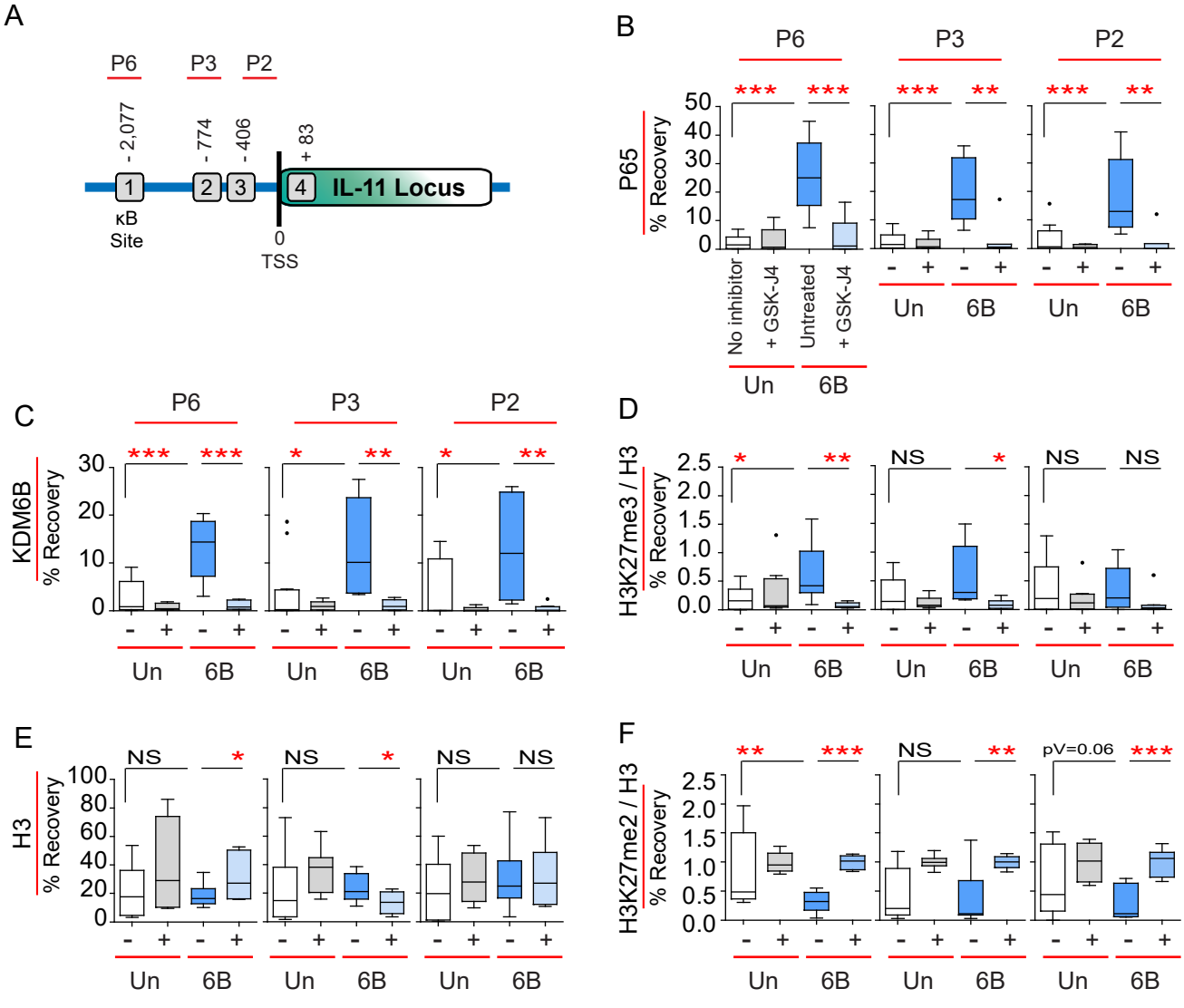
A
P6
P3
P2
- 2,077
- 774
- 406
+ 83
1
2
3
4
IL-11 Locus
κB Site
0 TSS
B
P6
P3
P2
P65 % Recovery
No inhibitor
+ GSK-J4
Untreated
+ GSK-J4
Un
6B
C
KDM6B % Recovery
D
H3K27me3 / H3 % Recovery
E
H3 % Recovery
F
H3K27me2 / H3 % Recovery
NS
pV=0.06

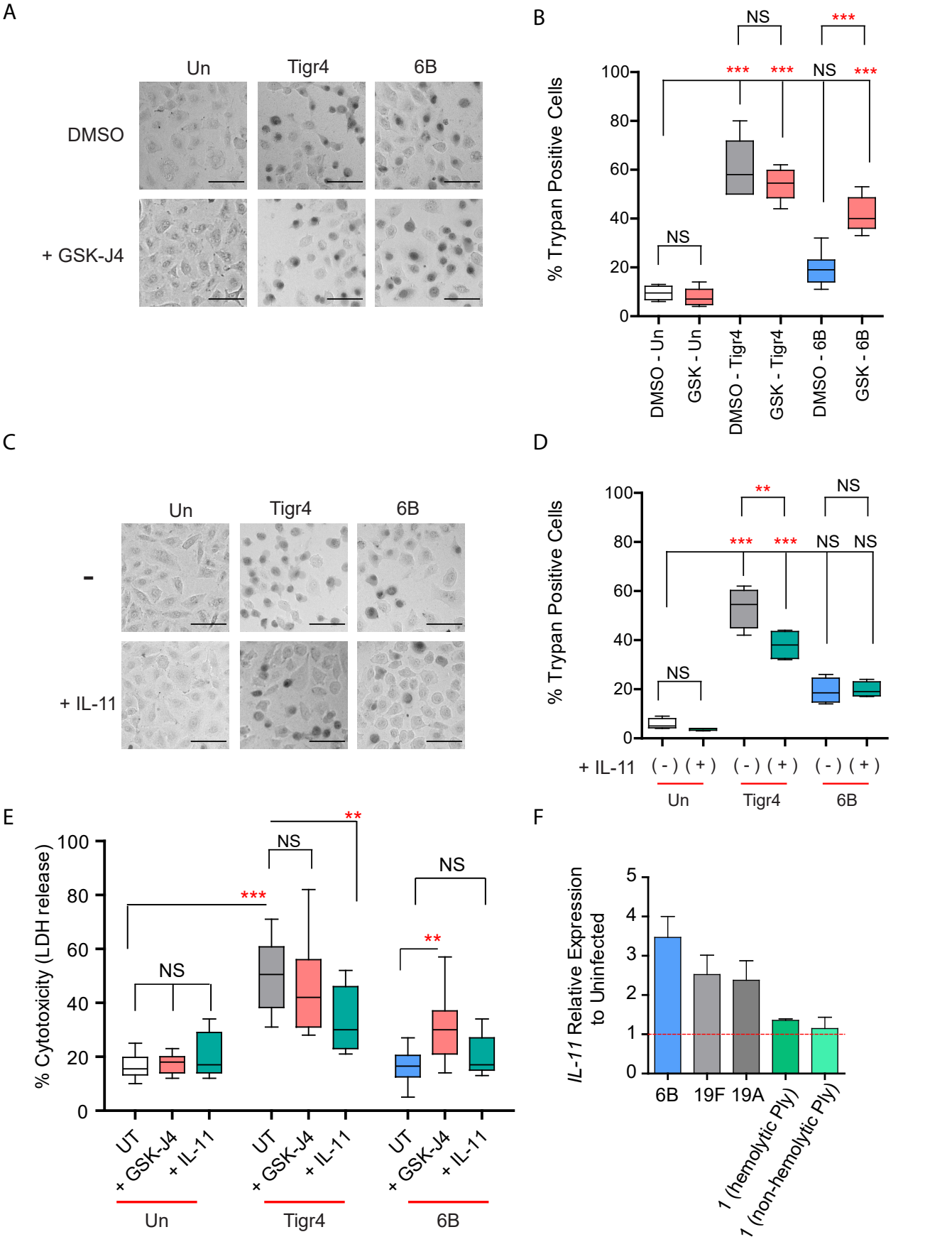
A
Un
Tigr4
6B
DMSO
+ GSK-J4
B
% Trypan Positive Cells
NS
***
DMSO - Un
GSK - Un
DMSO - Tigr4
GSK - Tigr4
DMSO - 6B
GSK - 6B
C
Un
Tigr4
6B
-
+ IL-11
D
% Trypan Positive Cells
**
+ IL-11
(-) (+)
Un
Tigr4
6B
E
% Cytotoxicity (LDH release)
UT
+ GSK-J4
+ IL-11
F
IL-11 Relative Expression to Uninfected
6B
19F
19A
1 (hemolytic Ply)
1 (non-hemolytic Ply)

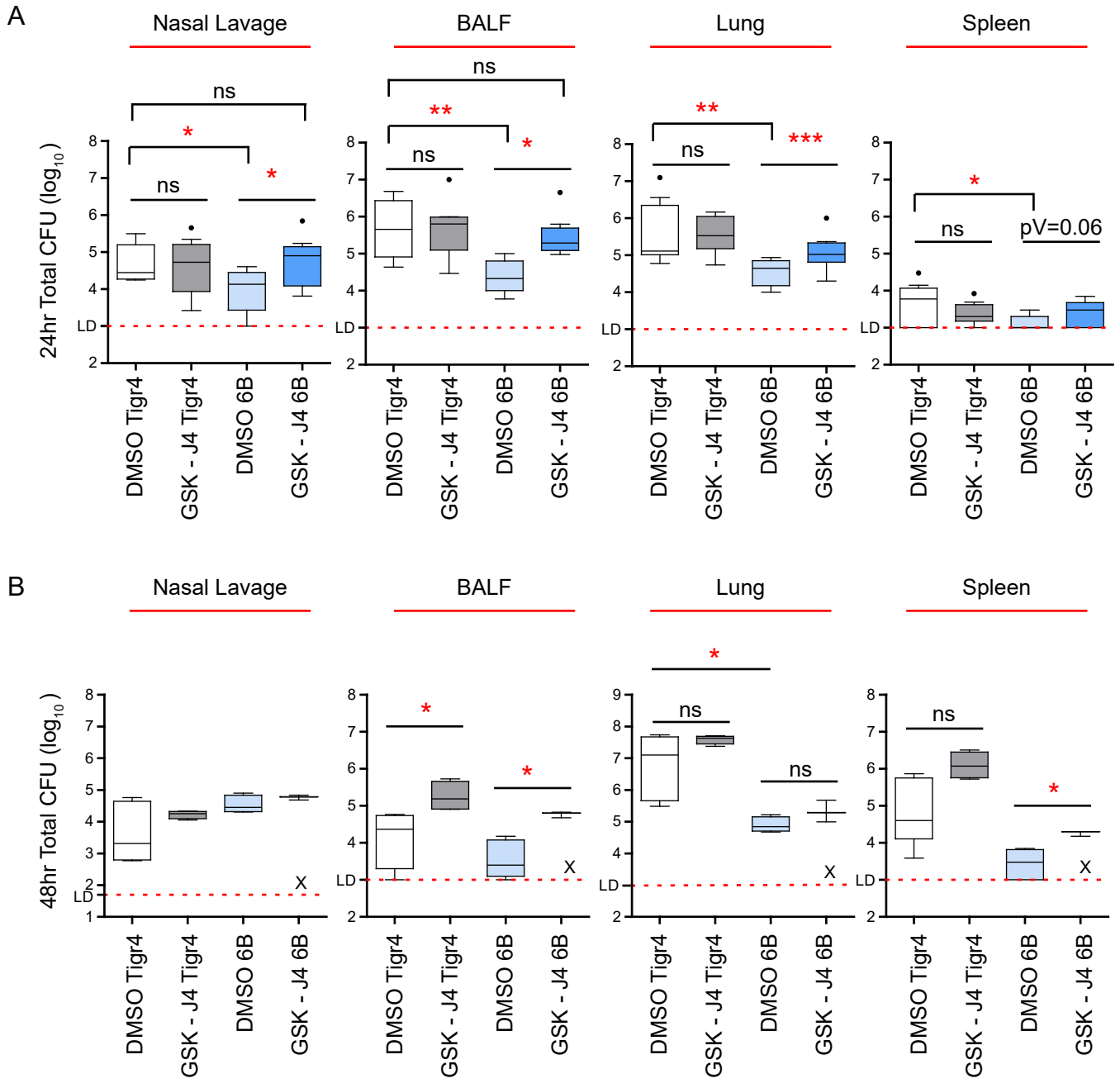
A
Nasal Lavage
BALF
Lung
Spleen
24hr Total CFU (log10)
ns
*
**
***
pV=0.06
LD
DMSO Tigr4
GSK - J4 Tigr4
DMSO 6B
GSK - J4 6B
B
48hr Total CFU (log10)
X